Theor Chem Acc (1999) 103:124–140
DOI 10.1007/s002149900042

Theoretical
Chemistry Accounts

Regular article

The Gaussian and augmented-plane-wave density functional method for ab initio molecular dynamics simulations

Gerald Lippert, Jürg Hutter, Michele Parrinello

Max-Planck-Institut für Festkörperforschung, Heisenbergstrasse 1, D-70569 Stuttgart, Germany

Received: 15 December 1998 / Accepted: 18 February 1999 / Published online: 14 July 1999

Abstract. A new algorithm for density-functional-theory-based ab initio molecular dynamics simulations is presented. The Kohn–Sham orbitals are expanded in Gaussian-type functions and an augmented-plane-wave-type approach is used to represent the electronic density. This extends previous work of ours where the density was expanded only in plane waves. We describe the total density in a smooth extended part which we represent in plane waves as in our previous work and parts localised close to the nuclei which are expanded in Gaussians. Using this representation of the charge we show how the localised and extended part can be treated separately, achieving a computational cost for the calculation of the Kohn–Sham matrix that scales with the system size N as $O(N \log N)$. Furthermore, we are able to reduce drastically the size of the plane-wave basis. In addition, we introduce a multiple-cutoff method that improves considerably the performance of this approach. Finally, we demonstrate with a series of numerical examples the accuracy and efficiency of the new algorithm, both for electronic structure calculations and for ab initio molecular dynamics simulations.

Key words: Gaussian basis – Augmented plane waves – Density functional method – Molecular dynamics

1 Introduction

The calculation of the electronic properties of large systems in the frame-work of density functional theory (DFT) [1] is a problem of great current interest to which much effort is being devoted. The more traditional and highly successful quantum chemistry methods use atom-localised functions expanded in Gaussians as their basis set. This approach can optimally exploit the properties of Gaussians, but finds a bottleneck in the calculation of the Hartree and exchange-correlation (XC) potentials. In order to circumvent this difficulty various remedies have been proposed. A popular solution has been to expand the density in an auxiliary basis set of atom-centred Gaussians, [2, 3]. Very recently, we and others have proposed using instead a plane-wave (PW) basis set to represent the density [4, 5]. In this basis the calculation of the Hartree potential is straightforward and by making use of fast Fourier transforms (FFT) the complexity of this part of the calculation becomes $O(N \log N)$, where N is the number of basis functions taken here as a measure of the system size. The Kohn and Sham (KS) potential can be represented in the real-space mesh associated with the FFT and we have devised convenient semianalytic recursion relations to calculate the matrix elements of the KS potential. In practice, if one were to apply this approach to an all-electron calculation the rapidly varying electron density close to the nuclei would require an impracticably large number of PW to be accurately represented. For this reason in Ref. [4] we used pseudopotentials which integrate out the core electrons and lead to a smoothly varying density, which can be expressed in a limited number of PW. The resulting algorithm is quite efficient in comparison with other methods, and makes it possible to treat periodic systems in a natural way; however, an important fraction of the computation time has to be devoted to the collocation of the density on the real-space FFT mesh and the evaluation of the KS potential matrix elements on the same mesh. This is particularly demanding for second-row and transition-metal elements, whose density varies rather rapidly, in spite of the use of pseudopotentials, and requires a dense FFT grid.

Here we propose a different representation of the density which further improves the performance of our new method. As in many band-structure methods, we find it convenient to divide the space into non overlapping localised spherical regions surrounding the atoms and the interstitial region.

The idea is that the interstitial density varies smoothly and is, therefore, easily representable in a PW basis, while the rapidly varying density close to the nuclei can be represented in terms of localised functions. Very recently Blöchl [6], in the framework of a new ingenious electronic

Correspondence to: M. Parrinello

structure method known as the projector augmented-wave (PAW) scheme, has shown how to circumvent some of the technical difficulties associated with the calculation of the XC potential and the Hartree term when the charge density is partitioned into a smooth and an atom-localised non-overlapping part. Here we will draw heavily on this work; however, our approach differs from the PAW scheme in many important ways. We represent the KS orbitals in Gaussians and not in augmented waves. This simplifies the calculation of many matrix elements and will in future allow easier implementation of linear scaling methods. We use a different procedure to partition the density into localised and smooth parts. Although we still use pseudopotentials, the present approach can be extended in a straightforward fashion to include fully the core electrons, thus leading to an all-electron scheme. In addition we present a multiple-cutoff method for the calculation of the KS matrix elements, which further enhances the performance of the present approach. The layout of the paper is as follows. In Sect. 2 we recall the essential features of the hybrid Gaussian and PW method that underlies our new approach. In Sect. 5 we introduce the new representation of the density and recall how the KS potential can be calculated following the PAW method. After that, we discuss how such a representation of the density can be obtained. In Sect. 3 we introduce our multiple-cutoff scheme. The functional form of the resulting energy functional is presented in Sect. 6: the corresponding formulae for the matrix elements and interatomic forces can be found in the Appendix. In a final section we present results of a series of test calculations and discuss various aspects of the performance of the method.

2 The hybrid Gaussian and PW density functional

In this section we want to recall the main features of the hybrid Gaussian and PW algorithm (GPW) proposed in Ref. [4]. which is the starting point for the present method. In the following we will refer to this method as the Gaussian and augmented-PW (GAPW) method.

The expression for the total electronic energy of a molecular or crystalline system in the KS formulation of DFT [1, 7, 8] is

$$E^{\mathrm{el}}[n] = E^{\mathrm{T}}[n] + E^{\mathrm{V}}[n] + E^{\mathrm{H}}[n] + E^{\mathrm{XC}}[n] \ , \tag{1}$$

where $E^{\mathrm{T}}[n]$ is the kinetic energy, $E^{\mathrm{V}}[n]$ the electronic interaction with the ionic cores, and $E^{\mathrm{H}}[n]$ and $E^{\mathrm{XC}}[n]$ are the electronic Hartree and XC energy, respectively.

Within the GPW approach the electronic density n is defined by its expansion in the basis functions

$$n(\mathbf{r}) = \sum_{\mu\nu} P_{\mu\nu}\varphi_\mu(\mathbf{r})\varphi_\nu(\mathbf{r}) \ , \tag{2}$$

with the density matrix $P_{\mu\nu}$. The $\varphi_\mu(\mathbf{r})$ are contracted Gaussian basis functions

$$\varphi_\mu(\mathbf{r}) = \sum_m C_{m\mu} g_m(\mathbf{r}) \ , \tag{3}$$

where $g_m(\mathbf{r})$ are the primitive Gaussians. In the numerical examples presented in Sect. 7 we shall use a basis of the response-function type [9].

The core electrons are eliminated from the calculation by introducing atomic pseudopotentials. The pseudopotential form chosen is the one designed by Goedecker and coworkers [10, 11] which is separable and norm-conserving and is based on Gaussians. Therefore, the contributions of the kinetic energy and the pseudopotential can be evaluated analytically within the Gaussian basis using recurrence relations [12].

To evaluate the density-dependent contributions $E^{\mathrm{H}}[n]$ and $E^{\mathrm{XC}}[n]$ the density is expanded in an auxiliary basis of PW

$$\check{n}(\mathbf{r}) = \frac{1}{\Omega} \sum_{|\mathbf{G}|<G_{\mathrm{C}}} n(\mathbf{G}) \mathrm{e}^{i\mathbf{G}\mathbf{r}} \ , \tag{4}$$

where Ω is the volume of the periodic cell and $E_C = \frac{1}{2} G_{\mathrm{C}}^2$ is the PW cutoff energy determining the number of wavevectors in the reciprocal grid. Starting from the reciprocal-space representation of the density the Hartree and the XC energies and potentials can be calculated straightforwardly by switching between real-space and reciprocal-space representations with the aid of FFT. Finally, the KS energy functional in the GPW approach has the form

$$\begin{aligned} E^{\mathrm{el}}[n] = & \sum_{\mu\nu} P_{\mu\nu} \left\langle \varphi_\mu(\mathbf{r}) \middle| -\frac{\Delta}{2} \middle| \varphi_\nu(\mathbf{r}) \right\rangle \\ & + \sum_{\mu\nu} P_{\mu\nu} \langle \varphi_\mu(\mathbf{r}) | V^{\mathrm{PP}}(\mathbf{r},\mathbf{r}') | \varphi_\nu(\mathbf{r}') \rangle \\ & + 4\pi\Omega \sum_{|\mathbf{G}|<G_{\mathrm{C}}} \frac{\check{n}^*(\mathbf{G})\check{n}(\mathbf{G})}{\mathbf{G}^2} \\ & + \int \mathrm{d}\mathbf{r} \ \check{n}(\mathbf{r}) \ E_{\mathrm{XC}}[\tilde{n}](\mathbf{r}) \ . \end{aligned} \tag{5}$$

the $G = 0$ term in the Hartree energy will be treated with the Ewald method [13, 14]. Note that the assumption of periodicity that is implied here does not limit the generality of this approach since isolated systems can be handled either with the approach in Refs. [15, 16] or in Refs. [17, 18], or by using an appropriate supercell.

Similar to the evaluation of the energy functional the calculation of the KS matrix elements is divided into two halves. The matrix elements of the kinetic energy and the pseudopotential can be integrated analytically using recursion relations, and the matrix elements of the Hartree and the XC potentials are calculated on the FFT mesh. The use of FFT enables us to combine the Hartree and the XC potentials into the KS potential. As a consequence these matrix elements need not be integrated separately.

On the level of Gaussian primitives the matrix elements of the KS potential are defined as

$$\langle g_m | V_{\mathrm{KS}} | g_n \rangle = \frac{1}{\Omega^2} \sum_{|\mathbf{G}|<G_{\mathrm{C}}} g_{mn}(-\mathbf{G}) V_{\mathrm{KS}}(\mathbf{G}) \ , \tag{6}$$

where Ω is the volume of the periodic cell and $g_{mn}(\mathbf{G})$ is the Fourier transform of the product of the two Gaussians $g_{mn} = g_m g_n$.

We showed in Ref. [4] that the construction of the PW representation of the density and the integration of the matrix elements of the KS potential can be carried out on the real-space Fourier grid. Instead of calculating the density directly in reciprocal space via the analytical Fourier transforms of the product Gaussians g_{mn}

$$n(\mathbf{G}) = \sum_{mn} \mathscr{P}_{mn} g_{mn}(\mathbf{G}) \quad , \tag{7}$$

where $\mathscr{P}_{mn}$ is the density matrix in terms of the Gaussian primitives, we first calculate the density on the real-space FFT mesh points $\mathbf{R}_\mathrm{i}$

$$n(\mathbf{R_i}) = \sum_{mn} \mathscr{P}_{mn} g_{mn}(\mathbf{R_i}) \tag{8}$$

and then Fourier transform the total density:

$$n(\mathbf{G}) = \frac{\Omega}{M} \sum_{\mathbf{R_i} \in \Omega} n(\mathbf{R_i}) \mathrm{e}^{-i\mathbf{G}\mathbf{R_i}} \quad , \tag{9}$$

where M is the number of gridpoints in the FFT mesh. In the case of the matrix elements we proceed in the reverse order. We first Fourier transform the KS potential

$$V_\mathrm{KS}(\mathbf{R_i}) = \frac{1}{\Omega} \sum_{|\mathbf{G}|<G_\mathrm{C}} V_\mathrm{KS}(\mathbf{G}) \mathrm{e}^{i\mathbf{G}\mathbf{R_i}} \quad , \tag{10}$$

and then integrate the matrix elements on the real-space FFT mesh:

$$\langle g_m | V_\mathrm{KS} | g_n \rangle = \sum_{\mathbf{R_i} \in \Omega} g_{mn}(\mathbf{R_i}) V_\mathrm{KS}(\mathbf{R_i}) \quad . \tag{11}$$

The main advantage of this real-space integration technique is that the product Gaussians in Eqs. (8) and (11) can be truncated outside their localisation region. This leads to a system-size-independent effort for each Gaussian product which cannot be achieved in reciprocal space. Therefore, by going from the reciprocal to the real-space formulation, the scaling of the algorithm is reduced from $O(N^2)$ to $O(N)$.

Equations (8) and (11) are both exact representations of the electron density and the matrix elements for the KS potential, respectively, if the discrete Fourier transform of the $g_{mn}(\mathbf{G})$ is used. However, the whole method is based on the assumption that the cutoff is chosen to be high enough to ensure that the PW basis is sufficiently large to describe the electron density properly. In this case, the replacement of the discrete by the analytic Fourier transform of g_{mn} results only in a minor approximation.

Although the real-space formulation leads to a linear scaling algorithm, it turned out in the actual calculations that in spite of the use of pseudopotentials, the cutoff needed for a converged calculation leads to an unfavorably high number of FFT gridpoints. Therefore, the real-space integration becomes the time-limiting step of the whole algorithm.

The GAPW approach presented in the following sections is designed to cure this deficiency. By changing the representation of the electronic density from a pure PW to an APW representation the cutoff and, as a consequence, the number of FFT gridpoints needed for the PW part of the density is drastically reduced.

3 The GAPW representation of the electron density

The wavefunctions and, as a consequence, the electron density of a molecular system exhibit different properties in different regions of space. In the binding region the density varies slowly while close to the nuclei it shows a strong variation. This is valid for all-electron calculations but is also true, although to a much lesser extent, for the pseudopotential approach.

This suggests that for an efficient representation of the density, different regions need to be represented in a different manner, a concept which is widely used in band-structure calculations. We thus assume for the time being that we can write the density as the sum of three contributions

$$n = \tilde{n} - \tilde{n}^1 + n^1 \quad , \tag{12}$$

where $\tilde{n}$ is smooth and distributed over all space, and

$$n^1 = \sum_A n_A^1 \tag{13}$$

$$\tilde{n}^1 = \sum_A \tilde{n}_A^1 \tag{14}$$

are sums of atom-centred contributions n_A^1 and $\tilde{n}_A^1$, which are hard and soft, respectively. We assume that in some regions U_A around the atoms, which do not overlap

$$U_A \cap U_B = \emptyset \quad \text{for } A \neq B \quad . \tag{15}$$

the relation

$$\tilde{n}(\mathbf{r}) = \tilde{n}_A^1(\mathbf{r}) \quad \text{for } \mathbf{r} \in U_A \tag{16}$$

is true, and therefore $\tilde{n}_A^1$ cancels the contributions of $\tilde{n}$ inside the atomic region U_A, which is replaced by the hard component n_A^1. Outside the atomic regions in the interstitial region, I, we assume that

$$\tilde{n}(\mathbf{r}) = n(\mathbf{r}) \quad \text{for } \mathbf{r} \in I \quad , \tag{17}$$

or, equivalently

$$n_A^1(\mathbf{r}) - \tilde{n}_A^1(\mathbf{r}) = 0 \quad \text{for } \mathbf{r} \in I \quad . \tag{18}$$

Note that this is automatically satisfied if n_A^1 and $\tilde{n}_A^1$ are entirely confined within the regions U_A, but this does not necessarily have to be true.

With this separation we can treat different regions of space in a different manner: $\tilde{n}$ is easily representable with small numbers of PW, while we can use localised Gaussians to represent n^1 and $\tilde{n}^1$.

We now collect the assumptions made to set up the GAPW representation of the electron density:

$$\begin{aligned} &n(\mathbf{r}) - \tilde{n}(\mathbf{r}) = 0 \quad \text{for } \mathbf{r} \in I \\ &n_A^1(\mathbf{r}) - \tilde{n}_A^1(\mathbf{r}) = 0 \quad \text{for } \mathbf{r} \in I \\ &\tilde{n}(\mathbf{r}) - \tilde{n}_A^1(\mathbf{r}) = 0 \quad \text{for } \mathbf{r} \in U_A \\ &n(\mathbf{r}) - n_A^1(\mathbf{r}) = 0 \quad \text{for } \mathbf{r} \in U_A \quad . \end{aligned} \tag{19}$$

Making use of these relations Blöchl [6] has demonstrated that the Hartree and XC functionals can be

separated into independent global and local contributions. The semilocal XC functionals $E_{\rm XC}[n]$ such as the local density approximation (LDA) or the general gradient approximation can be simply written as

$$E_{\rm XC}[n] = E_{\rm XC}[\tilde{n}] - \sum_A E_{\rm XC}[\tilde{n}_A^1] + \sum_A E_{\rm XC}[n_A^1] \ . \tag{20}$$

The first term can be calculated on the real-space grid of the FFT, while the other two are single-centre integrals that can be very accurately evaluated using atomic meshes.

More involved is the calculation of the Hartree term, which requires the introduction of appropriate localised screening densities expanded in a set of hard and soft Gaussians, respectively:

$$\begin{aligned} n_A^0 &= \sum_{\ell m} Q_A^{\ell m}\ g_A^{\ell m} \qquad n^0 = \sum_A n_A^0 \\ \tilde{n}_A^0 &= \sum_{\ell m} Q_A^{\ell m}\ \tilde{g}_A^{\ell m} \qquad \tilde{n}^0 = \sum_A \tilde{n}_A^0 \ . \end{aligned} \tag{21}$$

The $Q_A^{\ell m}$ are defined as

$$Q_A^{\ell m} = N q^{\ell m}\left[n_A^1 - \tilde{n}_A^1 + n_A^{\rm Z}\right] \ . \tag{22}$$

where $q^{\ell m}[n]$ is the multipole moment operator as defined in the Appendix, $n_A^{\rm Z}$ is the charge density of the ionic core at atom A, and N is a normalisation constant. These densities exactly cancel the electrostatic multipole moments of the one-centre densities and thus allow a separation of the contributions to the Hartree energy. The final result for the Hartree functional is

$$\begin{aligned} E_{\rm H}[n + n^{\rm Z}] = {} & E_{\rm H}\left[\tilde{n} + \tilde{n}^0\right] \\ & + \sum_A E_{\rm H}\left[n_A^1 + n_A^{\rm Z}\right] - \sum_A E_{\rm H}\left[\tilde{n}_A^1 + n_A^0\right] \\ & + E_{\rm H}[n^0] - E_{\rm H}[\tilde{n}^0] + \int {\rm d}\mathbf{r}\ V_{\rm H}\left[n^0 - \tilde{n}^0\right]\tilde{n} \ , \end{aligned} \tag{23}$$

where $E_{\rm H}[n]$ and $V_{\rm H}[n]$ denote the functionals

$$\begin{aligned} E_{\rm H}[n] &= \frac{1}{2}\iint {\rm d}\mathbf{r}\,{\rm d}\mathbf{r}'\frac{n(\mathbf{r})n(\mathbf{r}')}{|\mathbf{r}-\mathbf{r}'|} \\ V_{\rm H}[n](\mathbf{r}) &= \int {\rm d}\mathbf{r}'\frac{n(\mathbf{r}')}{|\mathbf{r}-\mathbf{r}'|} \ . \end{aligned} \tag{24}$$

As in the case of the XC functional, the Hartree functional in the GAPW formulation (Eq. 23) is separated into a global term that involves only smooth densities and local terms that involve short-ranged one-, two-, and three-centre integrals. Therefore, the global part can be calculated in the PW representation using a PW basis of modest size, while the local parts can be evaluated analytically in the Gaussian representation.

4 Construction of the GAPW density

The concepts that were introduced in the preceding section do not depend on the explicit form of the one-centre densities and it is not evident if or how the densities $\tilde{n}$, n^1, and $\tilde{n}^1$ that obey the conditions in Eq. (19) can be constructed. It is the aim of this section to show how these densities can be obtained within the GAPW approach.

4.1 The smooth density $\tilde{n}$

To construct the smooth density, $\tilde{n}$, the rapidly varying parts have to be eliminated from the original density, n. Since the density is defined by its expansion in basis functions φ_μ,

$$n = \sum_{\mu\nu} P_{\mu\nu}\ \varphi_\mu\varphi_\nu \ , \tag{25}$$

the rapid variations of φ_μ close to the nuclei will be reflected in n. When expanded in Gaussians, these variations require the use of strongly localised primitive Gaussians. As in Ref. [4] we will need a converged expansion of the Gaussians in PW and therefore the cutoff is forced up by the most localised primitives. It is thus natural and highly effective to smooth the basis functions by simply eliminating the most localised primitives in the response function expansion. Accordingly in the expression

$$\varphi_\mu = \sum_m C_{m\mu} g_m \tag{26}$$

we put to zero the coefficients $C_{m\mu}$ which correspond to the most localised Gaussians. This defines a smoothed basis function

$$\tilde{\varphi}_\mu = \sum_m \tilde{C}_{m\mu} g_m \ , \tag{27}$$

where

$$\begin{aligned} \tilde{C}_{m\mu} &= 0 \qquad \text{for } m = 1,\ldots,k \\ \tilde{C}_{m\mu} &= C_{m\mu} \qquad \text{for } m = k+1,\ldots,N_m \ . \end{aligned}$$

Clearly this smoothing affects only a localised region around the nuclei (Fig. 1). If we now define a density using the smooth functions $\tilde{\varphi}_\mu$ instead of the hard ones φ_μ

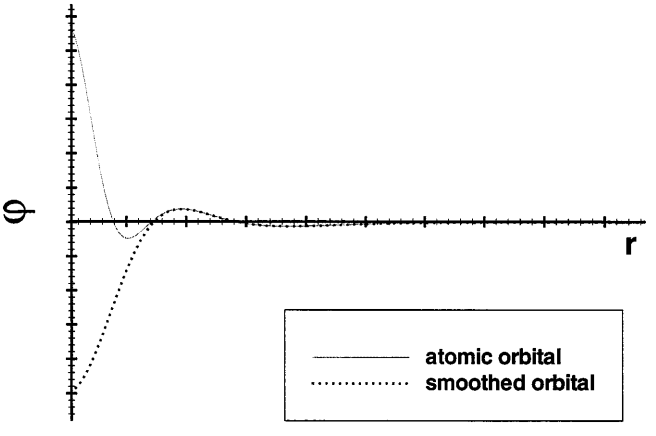

Fig. 1. Comparison between original basis function φ and smoothed basis function $\tilde{\varphi}$. The deviation is restricted to the region around the nuclei

$$\tilde{n} = \sum_{\mu\nu} P_{\mu\nu} \tilde{\varphi}_\mu \tilde{\varphi}_\nu \ , \tag{28}$$

this density can be expanded in PW with a much smaller cutoff, G_C,

$$\tilde{n} = \frac{1}{\Omega} \sum_{G<G_C} \tilde{n}(\mathbf{G}) e^{i\mathbf{G}\mathbf{r}} \ . \tag{29}$$

Furthermore, it is evident that this smooth density fulfils the requirement

$$n(\mathbf{r}) = \tilde{n}(\mathbf{r}) \quad \text{for } \mathbf{r} \in I \ , \tag{30}$$

if we define the atomic regions U_A as the regions around an atom A where $\tilde{\varphi}$ and φ are different, and I as the interstitial region outside the atomic regions. The condition (Eq. 15) is then a criterion for the number of primitives that can be eliminated. Starting from the most localised primitives, i.e. the ones with the highest exponents, we successively enlarge the atomic regions by leaving out primitives with smaller exponents. We can continue eliminating primitives as long as the overlap of the atomic regions is negligible.

4.2 The one-centre densities n^1 and $\tilde{n}^1$

After having defined the smooth global density, $\tilde{n}$, the procedure to construct the one-centre densities n^1 and $\tilde{n}^1$ is dictated by the conditions (Eq. 19) which require that the one-centre densities have to be locally identical to the global densities n and $\tilde{n}$. In order to achieve the goal of an efficient algorithm we need to impose the additional requirement that a one-centre density at a given atom is expanded only in basis functions centred at the same atom. Here we will discuss first the construction of the hard one-centre density, n^1, before applying the procedure to the construction of the smooth one-centre density, $\tilde{n}^1$.

We want to construct a density n^1_A centred at atom A, such that

$$n^1_A(\mathbf{r}) \approx n(\mathbf{r}) \quad \text{for } \mathbf{r} \in U_A \ , \tag{31}$$

and express such a density only in terms of a basis set centred on atom A. The problem of constructing n^1_A can be transformed into the finding functions χ_μ centred on A such that

$$\chi_\mu(\mathbf{r} - \mathbf{R}_A) \approx \varphi_\mu(\mathbf{r}) \quad \text{for } \mathbf{r} \in U_A \ , \tag{32}$$

whether φ_μ centred on A or not. If φ_μ is centred on A then we have

$$\chi_\mu = \varphi_\mu \ , \tag{33}$$

which in terms of the primitives reads

$$\chi_\mu = \sum_a C_{a\mu} g_a \ . \tag{34}$$

If φ_μ is not centred on A, its contribution to the density inside the region U_A is much smaller because φ_μ reaches inside U_A only with its tails. Since the tail is rather smooth it does not require much flexibility of the basis in which it is expanded. The orbital-like contracted basis functions at atom A, however, are not very well adapted to describe this smooth tail because of their oscillatory behaviour inside U_A. In contrast, the uncontracted primitives contained in the basis functions do not exhibit oscillations. Especially the more diffuse primitives with small exponents are able to reproduce the smooth tail correctly.

Therefore, we choose the primitive Gaussians g_a of the basis functions at atom A for the representation of the one-centre expansion of all the basis functions φ_μ. Consequently, the ansatz for the basis function approximation at atom A is

$$\chi_\mu = \sum_a C'_{a\mu} g_a \ . \tag{35}$$

Now the coefficients $C'_{a\mu}$ have to be determined so as to satisfy Eq. (32). We have already stated that the coefficients for the one-centre approximation of the basis functions located at the same atom are identical to the contraction coefficients of those basis functions

$$C'_{a\alpha} = C_{a\alpha} \ , \tag{36}$$

and therefore

$$\chi_\alpha = \sum_a C_{a\alpha} g_a = \varphi_\alpha \ . \tag{37}$$

The expansion coefficients $C'_{a\mu}$ for basis functions located at other atoms are determined in the spirit of the PAW method of Blöchl. We present here our realisation of the projection of the basis functions φ_μ onto the primitives g_a at atom A.

The purpose of the projection is to filter out from φ_μ at atom $M \neq A$ that part which is contained in U_A. To this effect we take a new set of Gaussians centred at A which serves as a projector basis $\{p_a\}$. The number of Gaussians in $\{p_a\}$ is equal to the number of primitives g_a. We choose the same set of exponents for all angular momenta. The smallest exponent is determined by the requirement that the Gaussian is just contained in U_A. Higher exponents, as customary, form a geometric progression.

Projecting the basis functions then yields

$$\langle p_b | \varphi_\mu \rangle = \sum_a C'_{a\mu} \langle p_b | g_a \rangle \ , \tag{38}$$

where we have inserted the desired result

$$\varphi_\mu(\mathbf{r}) \approx \sum_a C'_{a\mu} g_a(\mathbf{r}) \quad \text{for } \mathbf{r} \in U_A \ . \tag{39}$$

The coefficients $C'_{a\mu}$ can be obtained by inverting $\langle p|g\rangle$:

$$C'_{a\mu} = \sum_b \langle p|g\rangle^{-1}_{ab} \langle p_b | \varphi_\mu \rangle \ . \tag{40}$$

To simplify the notation we define a new set of projectors

$$\langle p'_a | = \sum_b \langle p|g\rangle^{-1}_{ab} \langle p_b | \ , \tag{41}$$

in order to write the coefficients as an overlap integral between the new projectors and the basis functions

$$C'_{a\mu} = \langle p'_a | \varphi_\mu \rangle \ . \tag{42}$$

In analogy to the total electron density

$$n = \sum_{\mu\nu} P_{\mu\nu}\varphi_\mu\varphi_\nu = \sum_{mn}\sum_{\mu\nu} C_{m\mu}P_{\mu\nu}C_{n\nu}g_m g_n \ . \tag{43}$$

we can not write the one-centre density n_A^1 as

$$n_A^1 = \sum_{\mu\nu} P_{\mu\nu}\chi_\mu\chi_\nu = \sum_{ab\in A}\sum_{\mu\nu} C'_{a\mu}P_{\mu\nu}C'_{b\nu}g_a g_b \ . \tag{44}$$

The constructed one-centre densities n_A^1 satisfy the condition

$$n_A^1(\mathbf{r}) = n(\mathbf{r}) \quad \text{for } \mathbf{r} \in U_A \tag{45}$$

only approximately. The quality of the approximation is, however, rather good due to the reason discussed previously, and in Sect. 7 we show with numerical tests that the error introduced is negligible.

In spite of the formal analogy of the total electron density and the one-centre density, not all of the basis functions and density matrix elements contribute to the one-centre density and the sum (Eq. 14) extends only formally over all pairs of indices, μ, ν. In fact, only those basis functions appear in the sum which overlap with the projectors at atom A, i.e. with the atomic region U_A. This ensures that the cost of calculating $n_A^1(\mathbf{r})$ is system-size independent.

In the same way as the one-centre densities n_A^1 are constructed the smooth one-centre densities can also be obtained:

$$\tilde{n}_A^1 = \sum_{\mu\nu} P_{\mu\nu}\tilde{\chi}_\mu\tilde{\chi}_\nu \ , \tag{46}$$

where

$$\tilde{\chi}_\mu = \sum_a \tilde{C}'_{a\mu}g_a \ . \tag{47}$$

Also in this case the one-centre expansion χ_μ of the basis functions φ_μ can be divided into two groups: the ones located at the same atom, and the others. Again, the first group can be described exactly

$$\tilde{\chi}_\alpha = \tilde{\varphi}_\alpha \quad (\alpha \in A) \ , \tag{48}$$

and the coefficients are identical to the contraction coefficients of the basis functions

$$\tilde{C}'_{a\alpha} = \tilde{C}_{a\alpha} \ . \tag{49}$$

For the second group the coefficients could again be determined by projection; however, there is no need for that. Since the hard and smooth basis functions coincide outside their atomic region U_M

$$\varphi_\mu(\mathbf{r}) = \tilde{\varphi}_\mu(\mathbf{r}) \quad \text{for } \mathbf{r} \notin U_M \tag{50}$$

and the atomic regions do not overlap; they coincide in particular inside the atomic regions of other atoms

$$\varphi_\mu(\mathbf{r}) = \tilde{\varphi}_\mu(\mathbf{r}) \quad \text{for } \mathbf{r} \in U_A,\ A \neq M \ . \tag{51}$$

The respective hard and soft one-centre expansions also coincide

$$\tilde{\chi}_\mu = \chi_\mu \qquad \tilde{C}'_{a\mu} = C'_{a\mu} \quad \text{for } A \neq M \ . \tag{52}$$

Therefore, the coefficients $\tilde{C}'_{a\mu}$ do not need to be determined by another projection, but can simply be taken from the one-centre expansion of the hard basis functions. In addition, it follows that the hard and the smooth one-centre densities

$$n_A^1 = \sum_{ab\in A}\sum_{\mu\nu} C'_{a\mu}P_{\mu\nu}C'_{b\nu}g_a g_b \tag{53}$$

$$\tilde{n}_A^1 = \sum_{ab\in A}\sum_{\mu\nu} \tilde{C}'_{a\mu}P_{\mu\nu}\tilde{C}'_{b\nu}g_a g_b \tag{54}$$

only differ from each other inside their atomic region, as was required by Eq. (19).

In this way we have succeeded in constructing the GAPW representation of the density

$$n = \tilde{n} - \tilde{n}^1 + n^1 \tag{55}$$

postulated in Eq. (12). We now have at our disposal two equivalent representations of the electron density, the linear combination of atomic orbitals representation

$$n = \sum_{\mu\nu} P_{\mu\nu}\varphi_\mu\varphi_\nu \tag{56}$$

and the GAPW representation

$$\tilde{n} - \tilde{n}^1 + n^1 = \frac{1}{\Omega}\sum_{G<G_C} \tilde{n}(\mathbf{G})\mathrm{e}^{i\mathbf{G}\mathbf{r}} - \sum_A\sum_{ab\in A}\sum_{\mu\nu} \tilde{C}'_{a\mu}P_{\mu\nu}\tilde{C}'_{b\nu}g_a g_b + \sum_A\sum_{ab\in A}\sum_{\mu\nu} C'_{a\mu}P_{\mu\nu}C'_{b\nu}g_a g_b \ , \tag{57}$$

which allow us to evaluate in the most appropriate way each of the various contributions to the KS functional (Eq. 5) from Sect. 2 with the modifications of the preceeding section.

Finally, we want to point out that, unlike in ordinary APW schemes [19], the atomic regions were only introduced as a concept to ensure that the subdivision of local and global terms is done correctly. They do not, however, appear explicitly in the functional, and they introduce no boundary conditions on basis functions, wavefunctions, or densities.

5 The multiple-cutoff method for the Fourier real-space integration and the PW expansion of the density

In G space the matrix elements of the KS potential are (see Eq. 6)

$$\langle g_m|V_{\mathrm{KS}}|g_n\rangle = \frac{1}{\Omega^2}\sum_{|G_i|<G_C} g_{mn}(-\mathbf{G})V_{\mathrm{KS}}(\mathbf{G}) \ . \tag{58}$$

While G_C is determined by the g_{mn} with the largest exponents, the g_{mn} with smaller exponents decay much

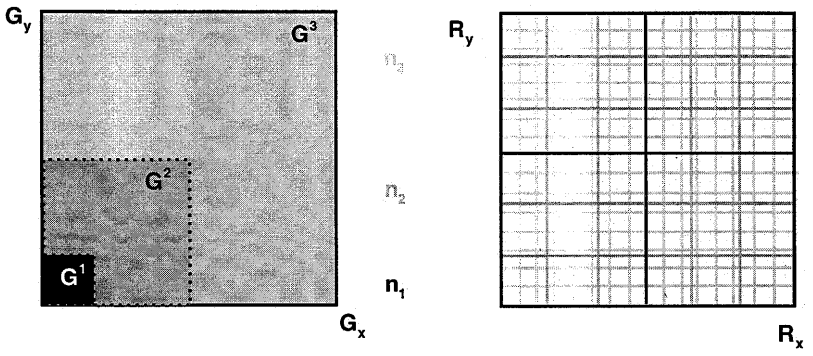

Fig. 2. The fast Fourier transform grids for the reciprocal-space and real-space representations when three grid levels are used. In reciprocal space each grid is a subgrid of the next highest level; therefore, different levels can be summed, multiplied, etc. with each other. In the real-space representation the grids are in general incommensurate

faster in G space and act as a filter. We can take advantage of this and in principle use for each g_{mn} a different cutoff E_C^{mn} determined by its exponent $\alpha_{mn} = \alpha_m + \alpha_n$. In real space this would lead to the use of a different mesh Ω_{mn} for different g_{mn}:

$$\langle g_m | V_{KS} | g_n \rangle = \sum_{R \in \Omega_{mn}} g_{mn}(\mathbf{R}) V_{KS}(\mathbf{R}) \quad . \tag{59}$$

This leads to big computational savings since for each matrix element we have to evaluate the same number of terms rather than having to use for all g_{mn} the very fine mesh needed to evaluate the largest exponent. Note that by varying E_C one obtains meshes in real space which are in general not simply related to one another (Fig. 2). One could use some interpolation scheme to go from V_{KS} in the finer mesh to the coarser one. In the spirit of this work we prefer to use the Fourier interpolation which amounts to calculating V_{KS}^{mn} as

$$V_{KS}^{mn}\mathbf{R} = \frac{1}{\Omega} \sum_{|G_i| < G_C^{mn}} V_{KS}\mathbf{G} e^{i\mathbf{GR}} \quad . \tag{60}$$

In fact, taking a different cutoff for each product g_{mn} is impractical because it involves a very large number of FFTs. For this reason we lump the g_{mn} in groups (Fig. 3) and within each group we use the same cutoff. In the test calculations reported later we have used between five and eight different meshes. The typical computational gain by the use of this multiple-cutoff method is a factor of 3–5.

Another part of the calculation that can profit from this scheme is the collocation of the density in the real-space grid, which is done to calculate $n(\mathbf{G})$ (see Eq. 8). To this effect we again lump the various contributions to $n(\mathbf{R})$ in groups according to the value of the exponent α_{mn}. For each group we use a different real-space mesh and perform an FFT with different cutoffs as was done earlier. The contributions in G space from the different groups of exponents are then summed together to obtain the total $n(\mathbf{G})$.

The cutoff values for the groups are determined by a new parameter, which we call the "relative cutoff" E_C^{rel}. We have shown [20] that for a given accuracy the cutoff energy for the expansion of a Gaussian with exponent α_{mn} is proportional to α_{mn}. This proportionality factor is E_C^{rel}:

$$E_C^{mn} = E_C^{rel} \alpha_{mn} \quad . \tag{61}$$

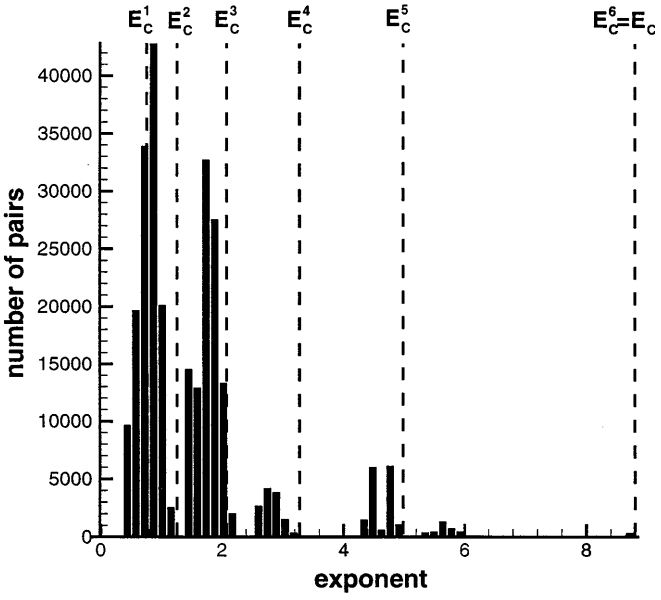

Fig. 3. Distribution of the number of Gaussians in the calculation of the density and the matrix elements of the Kohn–Sham potential depending on the exponents. The distribution was evaluated for a system of eight water molecules. The features of the distribution are nevertheless universal and depend only weakly on the system under consideration. The *broken lines* mark possible limits for the exponent intervals comprised in a cutoff level

The cutoff for each group of Gaussians is then given by the product of the biggest exponent in the group and the relative cutoff.

If the calculation of the Gaussian-pair functions in the density and the potential calculations are done on the same grids, the multiple-cutoff scheme can be regarded as a slight redefinition of $\tilde{n}(\mathbf{G})$.

6 The energy functional in the GAPW form

In this section we collect the modifications of the energy functional due to the GAPW representation of the electron density. The new functional, which is the defining expression of the GAPW method, has the form

$$E^{el}[\{\mathbf{R}_A\}, n] = E_T[n] + E_{V_{PP}}[n] + E_H[\tilde{n} + \tilde{n}^0] + \sum_A \{E_H[n_A^1 + n_A^Z] - E_H[\tilde{n}_A^1 + n_A^0]\}$$

$$- E_{\mathrm{H}}[\tilde{n}^0] + E_{\mathrm{H}}[n^0] + \int \mathrm{d}\mathbf{r} V_{\mathrm{H}}[n^0 - \tilde{n}^0]\tilde{n} + E_{\mathrm{XC}}[\tilde{n}] + \sum_A \{E_{\mathrm{XC}}[n_{\mathrm{A}}^1] - E_{\mathrm{XC}}[\tilde{n}_A^1]\} \quad , \qquad (62)$$

where n^0 and $\tilde{n}^0$ are the screening charge densities defined in Sect. 3 and n_A^Z is the charge density of the ionic core of atom A. It is easy to identify the contributions E_{T}. $E_{\mathrm{V_{PP}}}, E_{\mathrm{H}}[\tilde{n} + \tilde{n}^0]$ and $E_{\mathrm{XC}}[\tilde{n}]$ in the GAPW functional as the ones corresponding to the parts of the original functional (Eq. 5). The kinetic and pseudopotential energy contributions remain unchanged. As before, they will be evaluated analytically in the Gaussian representation. The important modification that has entered the Hartree and XC part is the substitution of the total density with the smooth global APW density. While the functional form and the procedure of the calculation remain the same, the amount of work is now greatly reduced due to the much smaller number of G vectors in the PW basis.

The additional parts of the GAPW functional that were absent in the original functional are the APW terms resulting from the one-centre contributions. These parts involve either sums of one-centre terms ($E_{\mathrm{H}}[n_A^1 + n_A^Z]$, $E_{\mathrm{H}}[\tilde{n}_A^1 + n_A^0], E_{\mathrm{XC}}[n_A^1], E_{\mathrm{XC}}[\tilde{n}_A^1]$) or two- and three-centre terms that decay very rapidly and can be screened efficiently ($E_{\mathrm{H}}[\tilde{n}^0] - E_{\mathrm{H}}[n^0], \int V_{\mathrm{H}}[n^0 - \tilde{n}^0]\tilde{n}$). All local contributions are evaluated in the Gaussian representation. While the contributions to the Hartree functional are integrated analytically with the aid of recurrence relations, the contributions of the XC functional are integrated numerically on Lebedev grids [21–23]. Due to their locality all these terms can be calculated with a very moderate computational effort. The gain in efficiency due to the reduction of the PW basis set size exeeds by far the additional cost of the local terms.

To conclude the presentation of the GAPW functional we recall the approximations inherent in the GAPW approach. One approximation is the finite size of the PW basis. As in pure PW schemes it is essential to ensure a converged calculation with respect to the PW cutoff. Since the quality of the PW basis depends only on one single parameter, the PW cutoff, it is easy to check the convergence in practical applications.

Another approximation is inherent in the one-centre expansion of the electronic density. Here, the main contributions arise from the on-centre terms, which are described exactly, while the contributions from other centres, which have to be approximated, are rather marginal. The quality of the expansion is limited by the variational freedom in the Gaussian basis of the respective atom; however, since the contributions from other centres consist only of the tails of the basisfunctions, a moderately sized basis set is enough to ensure an accurate description of the one-centre density.

As for all Gaussian-based methods, the influence of the basis on the result is by far the most severe. Compared to the incompleteness of the Gaussian basis set underlying the calculation, the errors introduced by the GAPW approach are negligible; however, by subsequently increasing the size of the Gaussian and the PW basis the GAPW method will, in the limit, give the exact result within the density functional framework.

Finally, we want to emphasize that all approximations in the GAPW approach can be thought of as slight redefinitions of the exact KS functional. Given the GAPW energy functional with its conceptual approximations, the matrix elements, the interatomic forces and all properties of the electronic structure are obtained as analytic derivatives of the energy functional. This implies in particular that the derived forces are consistent with the total energy, which is essential for the purpose of geometry optimisations and molecular dynamics simulations.

7 Test calculations

In the following subsections we report the results of a series of calculations, which were carried out to demonstrate the performance and reliability of the GAPW method. We start out with a study of the convergence behaviour of the method with respect to the PW cutoff. Then we report test calculations for several small molecules in comparison to other methods. We present a study of the scaling behaviour of the method for big systems, and finally we discuss a molecular dynamics simulation of an iron porphyrin system which serves as an example for a potential application of the method.

7.1 Convergence of the PW auxiliary basis

The main goal in the development of the GAPW method was to enhance the performance of the GPW method by reducing the number of PW needed for the expansion of the density and the KS potential; therefore, the first test calculations were carried out to clarify whether this goal had been achieved or not. We compared the convergence behaviour of the LDA total energy and the bond length of a water molecule with respect to the total PW cutoff for the GPW and the GAPW method (Fig. 4). The basis set we used had three functions per valence shell and two polarisation functions (TZV2P). One can see that both methods exhibit the same qualitative convergence behaviour, but for the GAPW method the curves are shifted towards lower cutoff energies. In the cutoff regions that correspond to reasonably well converged calculations one gains almost a factor of 3 by going from GPW to GAPW. Regarding the fact that the number of PW is proportional to $E_{\mathrm{C}}^{3/2}$ this amounts to a factor of 8 in the number of wave vectors, i.e. in the number of operations. Thus, it can be expected that the combined effect of the GAPW representation of the density and the multiple-cutoff method will remove the bottleneck of the FFT real-space integration from the method.

With the implementation of the multiple-cutoff method another parameter has been introduced: the relative cutoff $E_{\mathrm{C}}^{\mathrm{rel}}$. According to the discussion in Sect. 5 $E_{\mathrm{C}}^{\mathrm{rel}}$ is a universal quantity which is independent of the type of Gaussian basis set and the system under consideration. Once determined, it can be used in all calculations; therefore, the second test in this section is a study of the convergence of a calculation with respect to $E_{\mathrm{C}}^{\mathrm{rel}}$. As a test case we again took a water molecule with a

basis set of TZV2P type (Table 1). Starting from a value of 50 rydberg E_C^{rel} was reduced stepwise to a value of 15 rydberg. The LDA total energy, bond length, and bond angle are hardly affected until E_C^{rel} drops bellow 30 rydberg; however, one then sees a drastic effect between 20 and 15 rydberg, and below 15 rydberg the geometry optimisation failed to converge. This suggests a standard value for E_C^{rel} around 30 rydberg, which may be varied to higher or lower values in cases when high accuracy or high performance is demanded, respectively.

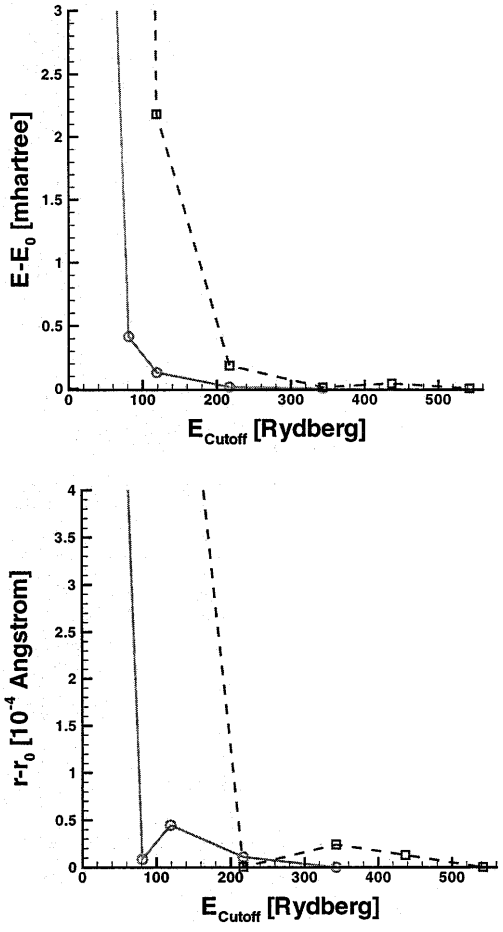

Fig. 4. Comparison of the convergence behaviour with respect to the cutoff energy E_{Cutoff} of the Gaussian and plane-wave (*GPW*) and Gaussian and augmented- PW (*GAPW*) methods. The differences in the total energy E [mhartree] and the bond length r [10^{-4} Å] relative to the equilibrium values of a water molecule are shown. The *full lines* correspond to the GAPW calculation and the *dashed lines* to the GPW calculation

7.2 Small molecules

The calculations presented in this section serve as a comparison between the GAPW method and several other methods with respect to the accuracy of the results. A series of calculations of structural properties of small molecules in the LDA was carried out. The differences in the methods under investigation consist mainly of the different types of basis functions which represent the density. The calculations with Gaussian94 [24] use only Gaussian-type functions while CPMD [25] is a pure PW scheme. NUMOL [26] on the other hand uses numerical grids and is therefore free from basis-sets. The Gaussian94 calculations are all-electron calculations, NUMOL uses a frozen-core approximation, while the GPW, GAPW, and CPMD calculations use the pseudopotentials of Goedecker and coworkers [10, 11]. The basis sets used in the GPW and GAPW calculations are atomic response function basis sets [9] with five exponents contracted to three s and three p functions (three s functions for H) and two polarisation functions with single exponents of d symmetry (p symmetry for H), corresponding to a triple zeta double polarisation (TZ2P) basis set in the quantum chemical jargon.

The most important result of the structure optimisations reported in Table 2 is the excellent agreement of the GPW and GAPW results. This confirms the arguments in Sect. 6 stating that the additional approximations inherent in the GAPW approach do not affect the accuracy of the method. Comparing the GAPW results with the results of the other methods gives satisfactory agreement, regarding the fact that the basis sets used

Table 1. Total energy (hartree), bond length (Å) and bond angle (°) of H_2O for different values of the relative cutoff energy E_C^{rel} (rydberg) for the multiple-cutoff method. The total cutoff for all calculations was 336 rydberg

E_C^{rel}	Total energy	R_{O-H}	∠HOH
50	−17.170071	0.9716	105.55
40	−17.170071	0.9716	105.55
30	−17.170082	0.9716	105.55
20	−17.170608	0.9714	105.62
15	−17.173410	0.9719	105.44

Table 2. Bond lengths (Å) [and angles (°)] of several small molecules obtained with different methods: plane wave (*PW*), Gaussian and PW (*GPW*), Gaussian and augmental *PW* (*GAPW*), Gaussian 94 (*G94*) [24] and NUMOL [26]

Molecule	GPW	GAPW	PW	G94 (6-311++G(3df,2p))	NUMOL
H_2	0.766	0.766	0.766	0.764	0.765
HF	0.935	0.936	0.933	0.930	0.932
H_2O	0.971 (105.6)	0.971 (105.6)	0.971 (104.9)	0.969 (105.1)	0.970 (105.0)
NH_3	1.022 (107.5)	1.022 (107.5)	1.022 (107.3)	1.021 (107.4)	1.021 (107.3)
CH_4	1.097	1.097	1.097	1.095	1.096
N_2	1.105	1.105	1.094	1.094	1.094
F_2	1.403	1.405	1.387	1.381	1.384
CO	1.132	1.133	1.126	1.126	1.127
CO_2	1.169	1.169	1.162	1.160	1.162

in the GAPW calculations are standard basis sets of moderate size that can also be employed in larger applications, whereas the basis sets used in the other calculations are at the upper limit of practicability. Further enlargement of the basis in the GAPW calculation would yield even better agreement of the results.

Besides the molecular geometries, vibrational frequencies and atomisation energies are most widely used for the comparison of different methods. Here, we report results for a selection of diatomic molecules (Tables 3, 4). For the comparison of the results for the harmonic frequencies we carried out calculations with Gaussian94 where we used two different basis sets to give an estimate of the influence of the basis on the results. The differences between the GPW and GAPW results indicate that the GPW calculations might not be fully converged. Especially the molecules containing O and F, which both need a relatively high cutoff in the GPW approach, exhibit strong deviations.

In contrast to the harmonic frequencies the atomisation energies of the GPW and the GAPW methods are in excellent agreement. This is due to the fact that the atomisation energies are energy differences, which converge much faster than absolute quantities. The results are also in good agreement with the PW calculations where the average deviation is 6 kcal/mol.

7.3 Big Systems

In the previous section the reliability of the GAPW method was studied. The tests reported there were essential to ensure that the application of the method leads to accurate results within the density functional framework. The method, however, was not designed for calculations of those small molecules, but for the efficient simulation of big systems. Since most of the relevant features of our approach only become significant for systems of intermediate and larger size we present here several studies with zeolite systems, where the system size ranges from 72 to 360 atoms, or from 936 to 6336 basis functions.

In the first study we examined the scaling behaviour of the computational cost of the GAPW method with zeolite systems that were composed of multiple copies of a unit cell of $Si_{24}O_{48}$ (Z1) with two different basis set types, namely a DZVP (13 functions/atom) and a TZV2P (22 functions/atom). In all calculations the LDA was used. The timings of the construction of the KS matrix are shown in Table 5. The DZVP calculation for the largest system, which is 5 times as big as the smallest one, takes about 5.5 times longer. For the TZV2P calculations the ratio of the system sizes of the biggest and the smallest system is 4 and the time ratio is 4.3. The numbers clearly prove that the scaling with system size of the computation time for the construction of the KS matrix is nearly linear.

Another aspect is the influence of the basis set type on the computational cost of a calculation. We carried out calculations of the zeolite system $Si_{24}O_{48}$ with four different basis sets of SZV, DZV, DZVP, and TZV2P quality, with a cutoff of 60 rydberg and the LDA functional (Table 6). The observation that can be made is that the computation time increases sublinearly with the number of basis functions. Doubling the size of the basis from SZV to DZV only requires 40% more computation time. This behaviour is due to the use of basis sets with shared exponents, which have the same number of primitives for the SZV, DZV, and TZV shells. This property can be optimally exploited in our analytical recursion scheme and our FFT real-space integrations. For the GAPW method this behaviour is essential since

Table 3. Harmonic frequencies (cm^{-1}) of several diatomic molecules obtained with different methods

Molecule	GPW	GAPW	G94 6-311G (2d,2p)	G94 6-311++G)3df,2p)
H_2	4204	4200	4207	4206
HF	3870	3939	4029	4008
N_2	2374	2375	2396	2407
F_2	1084	1045	1059	1062
CO	2194	2178	2186	2193

Table 4. Atomisation energies (kcal mol^{-1}) of several diatomic molecules obtained with different methods. The basis set superposition error (*BSSE*) in the GPW and GAPW calculations (< 1 kcal mol^{-1}) was checked and corrected with the "counterpoise" method [38]. The PW calculations are BSSE free

Molecule	GPW	GAPW	PW
H_2	157.1	157.1	154.3
HF	191.5	191.3	198.9
N_2	395.6	395.9	406.9
F_2	94.2	94.4	97.9
CO	357.9	357.9	362.9

Table 5. Computation time in seconds on an IBM 397 workstation for the construction and the diagonalisation (for the smaller systems) of the Kohn–Sham matrix of zeolite systems. N_{BF} denotes the number of basis functions and N_{el} the number of electrons in the system

Basis	System	N_{el}	N_{BF}	Construction	Diagonalisation
DZVP	$Si_{24}O_{48}$	384	936	110	84 (40%)
DZVP	$Si_{48}O_{96}$	768	1872	226	745 (77%)
DZVP	$Si_{72}O_{144}$	1152	2808	346	2635 (88%)
DZVP	$Si_{96}O_{192}$	1536	3744	466	
DZVP	$Si_{120}O_{240}$	1920	4680	611	
TZV2P	$Si_{24}O_{48}$	384	1584	187	309 (62%)
TZV2P	$Si_{48}O_{96}$	768	3168	383	
TZV2P	$Si_{72}O_{144}$	1152	4752	586	
TZV2P	$Si_{96}O_{192}$	1536	6336	802	

Table 6. Computation time in seconds on an IBM 395 workstation for the construction of the Kohn–Sham matrix of zeolite systems. N_{BF} denotes the number of basis functions in the system. Relative numbers are given in parentheses

Basis	N_{BF}	Construction
SZV	288 (1.0)	100 (1.0)
DZV	576 (2.0)	141 (1.4)
DZVP	936 (3.3)	210 (2.1)
TZ2VP	1584 (5.5)	353 (3.5)

we are able to use high-quality basis sets without spoiling the overall performance of the method.

As already stressed, the reason for the linear scaling of the KS matrix setup is the locality of the KS–Hamilton operator, which couples only basis functions that are located sufficiently close to each other in real space. With increasing system size the fraction of interacting basis-function pairs decreases. On the level of the matrix elements this leads to a sparse population of the overlap matrix, the KS matrix, and in principle, the density matrix. To obtain a quantitative description of the locality of the interactions we monitored the fraction of nonvanishing matrix elements for the case of a zeolite system with different basis sets (Table 7). The result is that for the system we studied, the overlap and the KS matrixes are indeed only sparsely occupied, while the density matrix has no vanishing elements. This seems to contradict the assumption of locality of the interactions, but it can be explained. The orthogonality constraint for the KS orbitals prevents a good localisation of the orbitals, thus leading to a long-range coupling of the basis functions in the density matrix. We expect the effect of the locality of the interactions on the occupation of the density matrix to be sensible only for systems that are much larger than the systems considered here.

7.4 The iron porphyrin–imidazole–carbon monoxide complex

To give an impression of the possibilities that the QUICKSTEP implementation of the GAPW method offers, we present an example for a potential application: a molecular dynamics simulation of the iron porphyrin–imidazole–carbon monoxide complex. This complex belongs to the class of metal-substituted tetrapyrrole ring complexes which constitute the active centres of a variety of biological enzymes. As a result of their importance in biochemistry these complexes have been very intensively studied in the past [27–29]. We have chosen the iron porphyrin system because of the very recent ab initio investigation of Rovira et al. [30] on the same system which was carried out with the PW code CPMD [25] and which can serve as a benchmark for the GAPW method. It has to be emphasized that we do not intend to gain any new insight into the system under investigation but to demonstrate the applicability of the GAPW method to this type of problem.

The iron porphyrin system is depicted in Fig. 5. Our heme model contains the porphyrin ring with the central iron atom to which the imidazole ligand and the CO molecule are attached from opposite sides. The imidazole plays the role of the histidine which normally connects the active centre to the rest of the protein. The simulation cell measures $15 \times 15 \times 12$ Å in agreement with Ref. [30]. We used the gradient-corrected functional of Becke [31] and Perdew [32]. In the work of Rovira et al. [30] an eight-electron pseudopotential with nonlinear core corrections was employed for iron. This circumvents the inclusion of the semicore electrons of the $2s$ and $2p$ shell that would force up the cutoff and the computational cost considerably. This problem with the semicore states does not appear with the GAPW method, since the inclusion of inner electron shells does not affect the cutoff and has only a minor influence on the computational cost. Therefore, we used a 16-electron pseudopotential for iron avoiding the complications of the nonlinear core corrections. The cutoff for the CPMD calculation was 70 rydberg for the wavefunction or 280 rydberg for the density while we used a density cutoff of 107 rydberg and 5 cutoff levels with a relative cutoff of 20 rydberg in the QUICKSTEP calculation. The quality of the atomic basis sets was chosen in accordance with the importance of the atom for the Fe—CO bond: $3s3p3d$ functions for Fe, $3s, 3p, 2d$ functions for the neighbours of Fe and for O, $2s2p1d$ for all other C and N, and $2s$ for H. The choices for the cutoff and the basis sets are the result of a series of test calculations and represent a comprimise between accuracy and efficiency. The results of a geometry optimisation given in Table 8 prove that the chosen parameters are able to reproduce the essential features of the system.

The molecular dynamics simulation was carried out with a parallel computer implementation of QUICKSTEP on eight nodes of a CRAY T3E. With this configuration one self-consistent-field (SCF) step takes 57 s on average; one molecular dynamics step 17 min. During each molecular dynamics step the electronic struc-

Table 7. Fraction of nonvanishing elements ($> 10^{-10}$) (in percent) of the overlap, the Kohn–Sham and the density matrix for a $Si_{36}O_{64}$ zeolite system. N_{BF} denotes the number of basis functions in the system

Basis	N_{BF}	Overlap	Kohn–Sham	Density
DZV	768	34	81	100
DZVP	1248	22	53	100
TZVP	1632	25	60	100

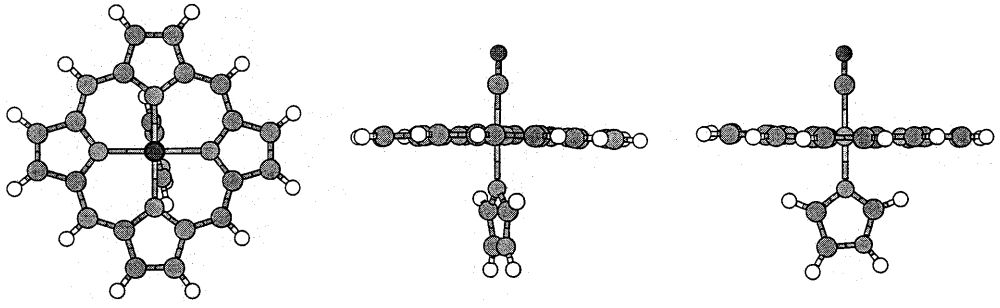

Fig. 5. The equilibrium structure of the iron porphyrin – imidazole – carbon monoxide [FeP(Im)(CO)] complex as obtained with the GAPW calculation

Table 8. The most important bond lengths (Å) and angles (°) of the iron porphyrin–imidazole–carbon monoxide complex obtained with different methods. N_{Im} denotes the N of the imidazole ring which is attached to Fe

	GAPW	PW [30]	Experiment [59]
R_{Fe-C}	1.74	1.72	1.77
R_{C-O}	1.17	1.17	1.12
∠FeCO	179	180	179
R_{Fe-N}	2.02	2.02	2.02
$R_{Fe-N_{Im}}$	2.05	2.07	2.10

ture is optimised, the interatomic forces are calculated, and the atomic coordinates and velocities are updated according to a standard velocity Verlet algorithm. A timestep corresponds to 0.97 fs. The system was propagated over a period of 2.2 ps at an average temperature of 291.1 K. Figure 6 shows the time evolution of the total energy, the total potential energy, which is composed of the total electronic energy and the interaction of the ionic cores, and of the temperature. The total energy is the sum of the kinetic energy of the nuclei and the total potential energy. This quantity should be conserved during the simulation. Its variations are a measure for the quality of the simulation. The reference quantity for the variations are the variations in the total potential energy. From the middle graph in Fig. 6 one can conclude that the total energy can be regarded as constant since the variations are 2 orders of magnitude less that those of the total potential energy.

Furthermore, it is obvious from Fig. 6 that the total energy has no drift. This implies that no energy is taken into or out of the system due to numerical inaccuracy, which would lead to artefacts in the dynamics. Another indicator for the same fact is the good conservation of the temperature.

After having verified that the molecular dynamics run satisfied the usual criteria we briefly summarise the results. As in Ref. [30] we concentrate on the dynamic behaviour of the Fe—CO unit; therefore, we define the angles which describe the orientation of the Fe—CO unit as in Fig. 7. The dynamics of these angles and the corresponding bond lengths are depicted in Fig. 8 and are compared to the results of the CPMD calculation. The distribution of the angles during the molecular dynamics run is shown in Fig. 9.

Given the differences of the pure PW approach and the GAPW method concerning the energy functional, the basis functions, the pseudopotentials, the timestep in the molecular dynamics, etc., the results agree remarkably well. The characteristics of the dynamic evolution of the quantities that were monitored are the same in both calculations. According to the small differences in the equilibrium structures the average values of the bond length are slightly shifted. A frequency analysis of the bond stretching resulted in satisfactory agreement within some ten wavenumbers. The dynamics of the angles deviates somewhat. The QUICKSTEP calculation contains more oscillations with larger amplitude, that lead to broader tails in the distributions; however; the coarse structure of the angular distributions in Fig. 9 gives a

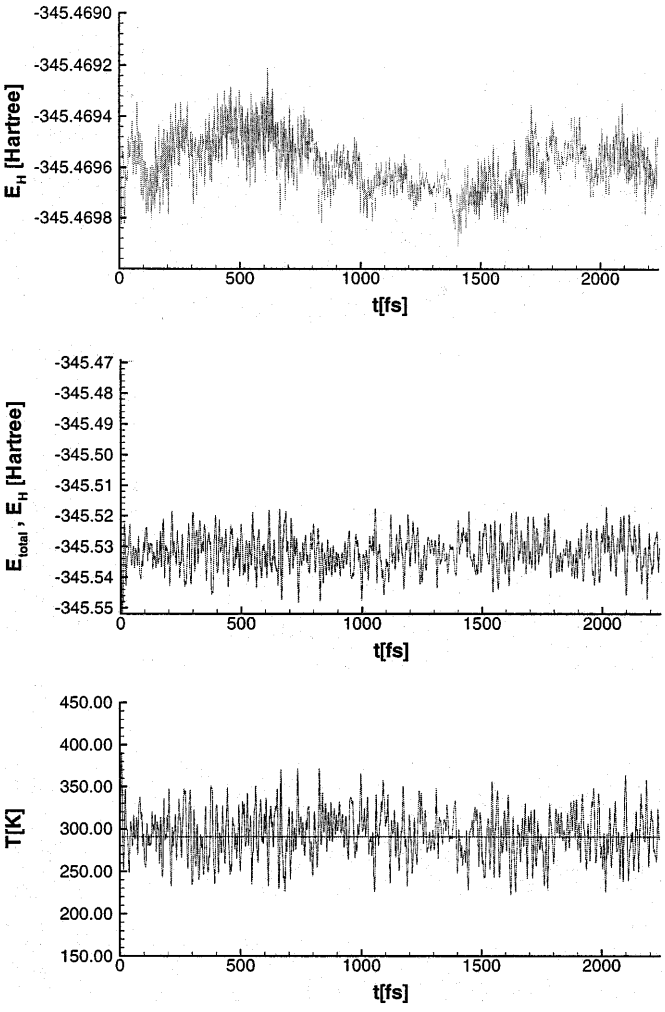

Fig. 6. The *upper graph* shows the time evolution of the total energy (E_H) of the FeP(Im)(CO) complex during the molecular dynamics simulation. In the *middle graph* the total energy (E_H, *upper curve*) is shown in relation to the total potential energy (E_{total}, *lower curve*). The *lower graph* shows the time evolution of the temperature. The mean value of the temperature (291.1 K) is marked

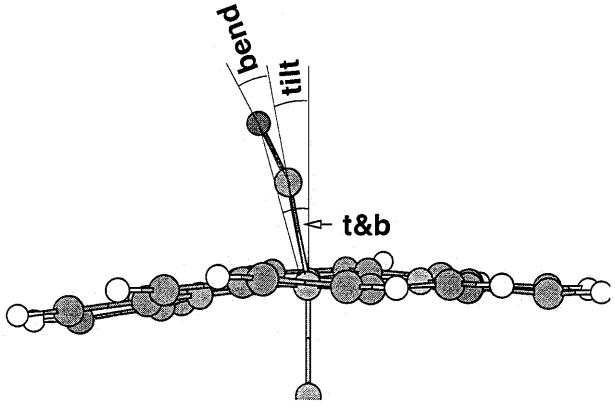

Fig. 7. Definition of the angles describing the Fe—CO unit: *tilt* is the angle of the Fe—C bond with the normal vector of the plane defined by the four nitrogens; *bend* is the angle of the Fe—C bond with the C—O bond; *t&b* is the angle of the difference vector of the Fe and O position with the normal vector of the nitrogen plane

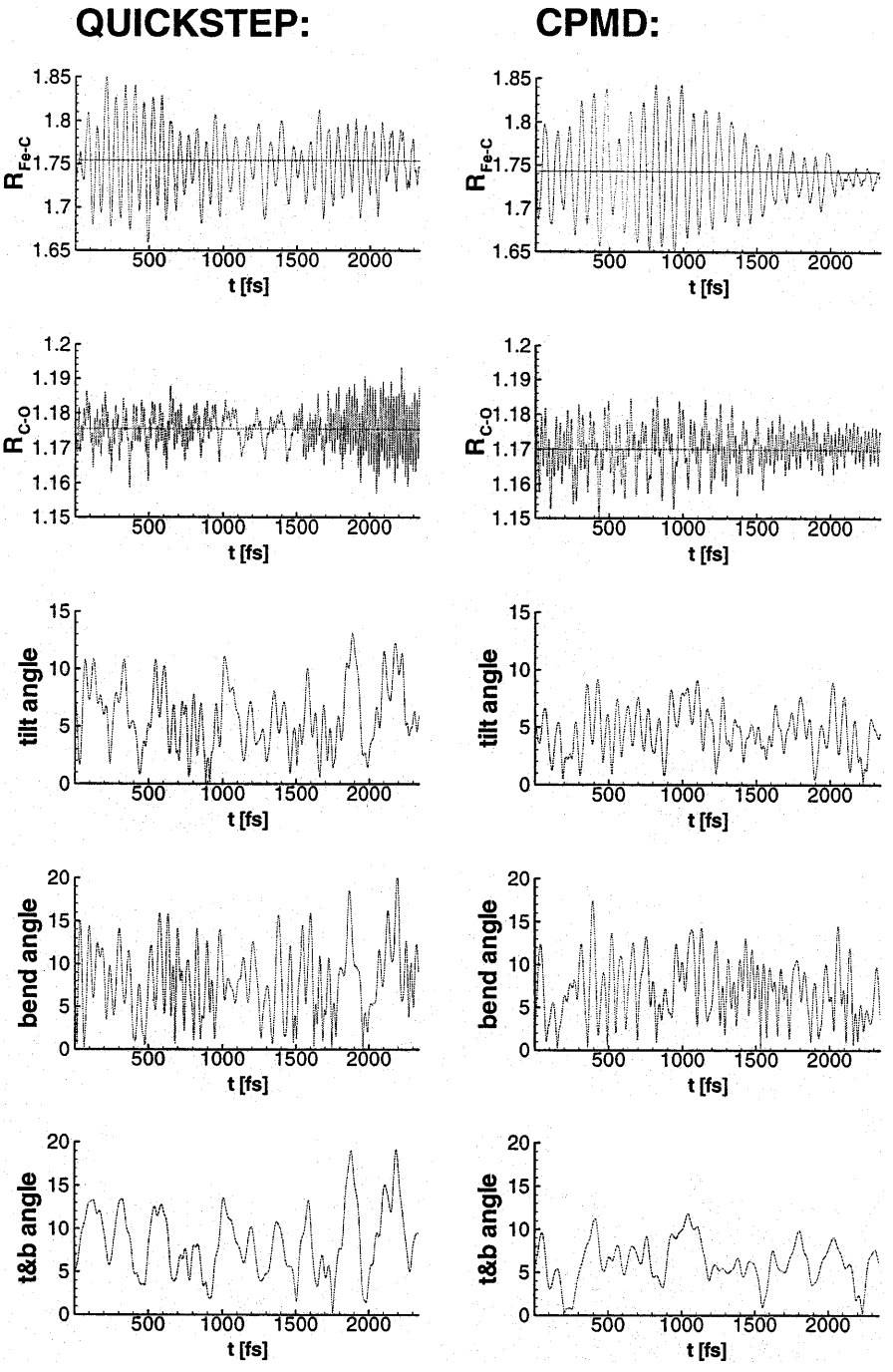

Fig. 8. Comparison of the dynamics of the bond lengths (Å) and angles (°) of the Fe—CO unit. On the *left side* are the results of the QUICKSTEP calculation, on the *right side* those of the CPMD calculation. The average values of the bond lengths are marked. The angles are defined in Fig. 7

hint that the length of the simulation does not allow sufficiently good statistics in order to make a quantitative comparison.

Summarising the discussion we can say that both methods lead to qualitatively equivalent results. In contrast to Ref. [30] we did not perform an analysis of the electronic structure of the complex. Nevertheless, such an analysis can be carried out using the GAPW method and, due to the use of localised basis functions, is even more straightforward than in the case of a pure PW scheme.

Finally we compare the computational resources needed for both methods. The computation time per femtosecond simulation time was 6700 s in the case of the CPMD run and 8400 s in the case of the QUICKSTEP run. This is an encouraging result for the GAPW method considering the fact that CPMD was optimised over a period of 10 years and scales almost perfectly on parallel computers while the QUICKSTEP implementation is hardly optimised for parallel computing and scales rather badly. Concerning the memory requirements QUICKSTEP is superior to CPMD. While the CPMD run had to be performed on 32 nodes of a CRAY T3E with 128 Mbyte each, the QUICKSTEP run could fit on only four nodes of the same type.

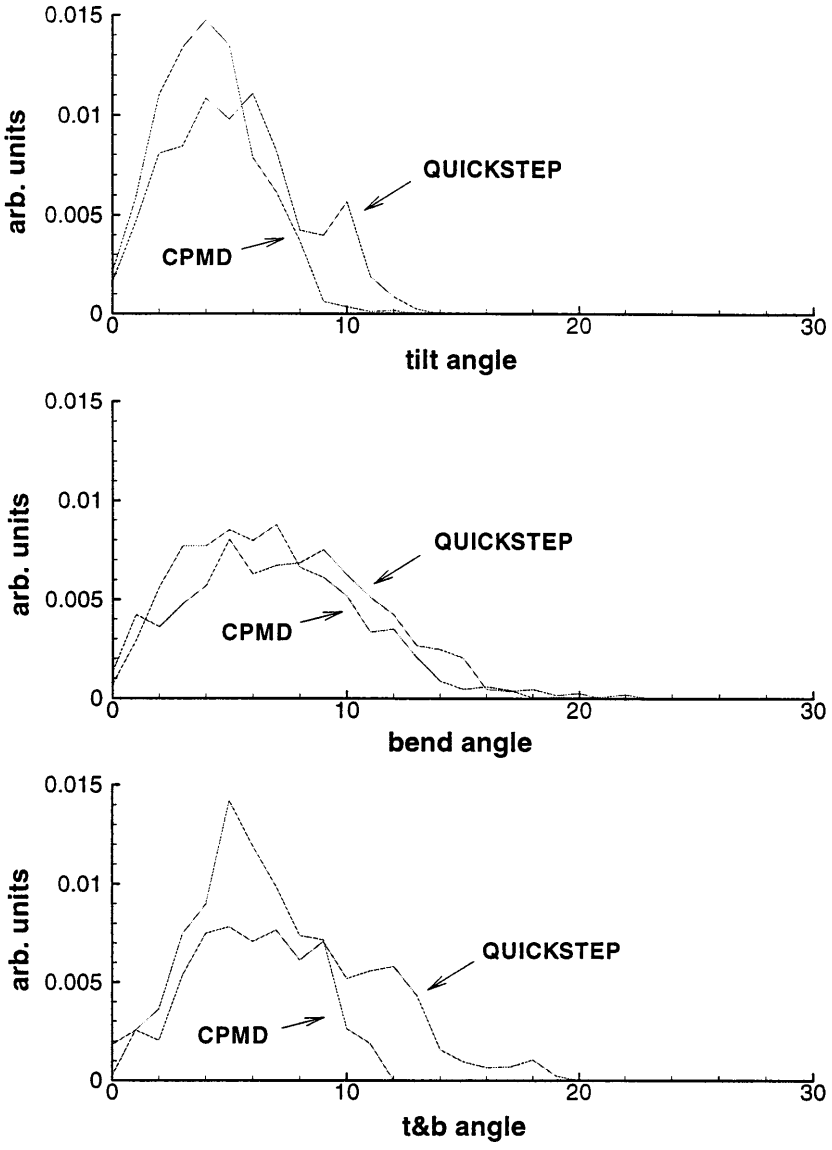

Fig. 9. Distribution of the tilt (*top*), bend (*centre*), and t&b (*bottom*) angles (°) during the molecular dynamics run with QUICKSTEP and CPMD. The angles are defined in Fig. 7

8 Conclusions

We have presented the GAPW method and discussed in detail the theoretical and algorithmic principles of the method. Starting from the GPW approach we substituted the PW auxiliary basis for the electron density by an APW auxiliary basis which besides plane waves relies on Gaussians. Therefore, the electron density, the XC potential, and the Coulomb potential can be separated into a smooth nonlocal contribution expanded in PW and local contributions that can be described in Gaussians and which can thus be treated analytically. The gain in efficiency due to the elimination of the hard contributions in the PW expansion of the density, resulting in a reduction of the number of wavevectors by a factor of about 5, is much greater than the additional effort for the Gaussian contributions. The $O(N \log N)$ scaling behaviour, which was the essential feature of the GPW method, is not affected by the transition to the GAPW approach.

The tests we performed demonstrate that the GAPW method is on the same level of accuracy and reliability as established DFT methods. In addition, the GAPW approach contains several desirable features which make it superior to pure PW methods and methods based only on localised basis functions. Like pure PW methods the GAPW method incorporates periodic boundary conditions in a natural way, making it especially suited for the simulation of condensed phases. However, since all important quantities are described in Gaussian-type orbitals the memory requirements of the algorithm are considerably lower than in pure PW schemes. Furthermore, in contrast to PW methods, the GAPW method is not sensitive to empty regions of space. Therefore, isolated systems can be simulated straightforwardly without having to worry about the vacuum separating the periodic replica of the system. The softness of pseudopotentials, being essential for the cutoff in pure PW schemes, is not crucial within the GAPW method, since the pseudopotential influences the hardness of the density only in

the core regions that are not included in the PW expansion, and the pseudopotential itself is treated analytically. Furthermore, it is possible to include the semicore states, which enables us to deal with transition metals, and even all-electron calculations can be performed.

The big advantage of the GAPW approach in comparison with methods based only on localised functions is the efficient calculation of the nonlocal part of the Hartree functional in the PW representation in reciprocal space. Using the APW ansatz for the electron density and the multiple-cutoff method we could speed up considerably the calculation of the PW representation of the density and the matrix elements of the KS potential. In contrast to methods based on localised functions, there is no fitting procedure involved in the representation of the density in the auxiliary basis. Another advantage of the GAPW approach is the combination of the Coulomb and the XC potential into the KS potential, that allows a combined integration of the matrix elements. In traditional methods the integration of the XC part has to be done numerically while the Coulomb part is done analytically.

The GAPW method was developed to make the ab initio simulation of very large systems of several hundreds of atoms feasible; therefore, the focus was set on the scaling behaviour of the method. The GAPW method is a major step in the direction of methods that scale linearly with the size of the system. The essential parts of the algorithm for the calculation of the KS matrix scale linearly or as $O(N \log N)$. A problem that needs to be addressed in the future is the update of the density matrix in the SCF procedure. The diagonalising of the KS matrix scales as N^3 and becomes the time-limiting step for larger systems. To achieve a more favourable scaling, methods along the direction of those proposed in the literature [33–37] have to be evaluated.

To further increase the scope of accessible system sizes we plan to use the GAPW method as part of a so-called ''embedding'' method. In this method only the central part which is chemically active is described quantum mechanically while the surroundings of the active centre are described classically. In this way sterical and electrostatic effects of the environment can be included in the simulation. The use of such methods will allow us to treat system sizes of several thousands of atoms in the near future.

Appendix: Matrix elements and interatomic forces in the GAPW formulation

In this Appendix we give the expressions for the matrix elements of the KS matrix and the gradients of the total energy with respect to the atomic positions. Since these formulae result from straightforward functional derivatives of the energy functional they are given without proof.

We start with the expression for the KS matrix elements. These are defined by

$$(\mathscr{H}_{\mathrm{KS}})_{\mu\nu} = \frac{\mathrm{d}}{\mathrm{d}P_{\mu\nu}} E^{\mathrm{el}} \ , \tag{A1}$$

where

$$\begin{aligned}\frac{\mathrm{d}}{\mathrm{d}P_{\mu\nu}} E[n, \nabla_i n, \ldots] &= \int \mathrm{d}\mathbf{r} \frac{\delta E[n, \nabla_i n, \ldots]}{\delta n(\mathbf{r})} \frac{\partial n(\mathbf{r})}{\partial P_{\mu\nu}} \\ &= \int \mathrm{d}\mathbf{r} \left\{ \frac{\partial E[n, \nabla_i n, \ldots]}{\partial n(\mathbf{r})} \right. \\ &\qquad \left. + \sum_i \nabla_i \frac{\partial E[n, \nabla_i n, \ldots]}{\partial \nabla_i n(\mathbf{r})} + \cdots \right\} \frac{\partial n(\mathbf{r})}{\partial P_{\mu\nu}} \ , \end{aligned} \tag{A2}$$

and n is one of the densities $n, \tilde{n}, n^1, \tilde{n}^1, n^0, \tilde{n}^0$. The resulting matrix elements are

$$\begin{aligned}(\mathscr{H}_{\mathrm{KS}})_{\mu\nu} = &\left\langle \varphi_\mu \middle| -\frac{\Delta}{2} \middle| \varphi_\nu \right\rangle \\ &+ \left\langle \varphi_\mu(\mathbf{r}) \middle| V_{\mathrm{loc}}^{\mathrm{PP}}(\mathbf{r}) \delta(\mathbf{r} - \mathbf{r}') + V_{\mathrm{nl}}^{\mathrm{PP}}(\mathbf{r}, \mathbf{r}') \middle| \varphi_\nu(\mathbf{r}') \right\rangle \\ &+ \left\langle \tilde{\varphi}_\mu \middle| V_{\mathrm{H}}[\tilde{n} + \tilde{n}^0] + V_{\mathrm{XC}}[\tilde{n}] \middle| \tilde{\varphi}_\nu \right\rangle_{\Omega_{\mathrm{FFT}}} \\ &+ \left\langle \tilde{\varphi}_\mu \middle| V_{\mathrm{H}}[n^0 - \tilde{n}^0] \middle| \tilde{\varphi}_\nu \right\rangle + \sum_{A\ell m} q^{\ell m}[\chi_\mu \chi_\nu - \tilde{\chi}_\mu \tilde{\chi}_\nu] \\ &\times \left\{ \int_{\Omega_{\mathrm{FFT}}} V_{\mathrm{H}}[\tilde{n} + \tilde{n}^0] \tilde{g}_A^{\ell m} + \int V_{\mathrm{H}}[\tilde{n}] (g_A^{\ell m} - \tilde{g}_A^{\ell m}) \right. \\ &\quad + \sum_{A'} \int V_{\mathrm{H}}[n_{A'}^0] g_A^{\ell m} - \sum_{A'} \int V_{\mathrm{H}}[\tilde{n}_{A'}^0] \tilde{g}_A^{\ell m} \\ &\quad \left. + \int V_{\mathrm{H}}[\tilde{n}_A^1 + n_A^0] g_A^{\ell m} \right\} \\ &+ \sum_A \left\langle \chi_\mu \middle| V_{\mathrm{H}}[n_A^1 + n_A^{\mathrm{Z}}] \middle| \chi_\nu \right\rangle \\ &- \sum_A \left\langle \tilde{\chi}_\mu \middle| V_{\mathrm{H}}[\tilde{n}_A^1 + n_A^0] \middle| \tilde{\chi}_\nu \right\rangle \\ &+ \sum_A \left\langle \chi_\mu \middle| V_{\mathrm{XC}}[n_A^1] \middle| \chi_\nu \right\rangle_{\Omega_{\mathrm{A}}} \\ &- \sum_A \left\langle \tilde{\chi}_\mu \middle| V_{\mathrm{XC}}[\tilde{n}_A^1] \middle| \tilde{\chi}_\nu \right\rangle_{\Omega_{\mathrm{A}}} \ . \end{aligned} \tag{A3}$$

The indices Ω_{FFT} and Ω_{A} denote integration on the FFT grid or on atomic Lebedev grids, respectively. All other integrals are evaluated analytically. The term $q^{\ell m}[n]$ denotes the multipole moments of a charge distribution n

$$q^{\ell m}[n] = \frac{4\pi}{2\ell + 1} \int \mathrm{d}\mathbf{r}' n(\mathbf{r}') \mathbf{r}'^{\ell} S^{\ell m}(\mathbf{r}') \ , \tag{A4}$$

where $S^{\ell m}$ are the real linear combinations of the spherical harmonics

$$\begin{aligned} S^{\ell 0} &= Y^{\ell 0} \\ S^{\ell m} &= \frac{1}{\sqrt{2}} \left(Y^{\ell m} + Y^{\ell -m} \right) \\ S^{\ell -m} &= \frac{1}{i\sqrt{2}} \left(Y^{\ell m} - Y^{\ell -m} \right) \ . \end{aligned} \tag{A5}$$

The interatomic forces are defined by the gradient of the total energy with respect to the atomic positions:

$$\mathbf{F}_A = -\frac{\mathrm{d}}{\mathrm{d}\mathbf{R}_A}E^{\mathrm{tot}}[\{\mathbf{R}_B\},n] = -\frac{\partial}{\partial\mathbf{R}_A}E^{\mathrm{tot}}(\{\mathbf{R}_B\}) - \sum_{n\in\{n,\tilde{n},n^1,\tilde{n}^1,n^0,\tilde{n}^0\}}\int \mathrm{d}\mathbf{r}\frac{\delta E[n,\nabla_i n,\ldots]}{\delta n(\mathbf{r})}\frac{\partial n(\mathbf{r})}{\partial\mathbf{R}_A} \quad . \tag{A6}$$

In the case of the kinetic energy and the pseudopotential energy this definition leads to the expression

$$\begin{aligned}
&\frac{\mathrm{d}}{\mathrm{d}\mathbf{R}_A}(E_{\mathrm{T}}+E_{\mathrm{PP}})\\
&\quad= 2\sum_{\mu\nu}P_{\mu\nu}\left\langle\varphi_\mu(\mathbf{r})\middle|-\frac{\Delta}{2}\middle|\nabla_{\mathbf{R}_A}\varphi_\nu(\mathbf{r})\right\rangle\\
&\qquad+2\sum_{\mu\nu}P_{\mu\nu}\left\langle\varphi_\mu(\mathbf{r})\middle|V_{\mathrm{loc}}^{\mathrm{PP}}(\mathbf{r})\middle|\nabla_{\mathbf{R}_A}\varphi_\nu(\mathbf{r})\right\rangle\\
&\qquad+2\sum_{\mu\nu}P_{\mu\nu}\left\langle\varphi_\mu(\mathbf{r})\middle|V_{\mathrm{nl}}^{\mathrm{PP}}(\mathbf{r},\mathbf{r}')\middle|\nabla_{\mathbf{R}_A}\varphi_\nu(\mathbf{r}')\right\rangle\\
&\qquad+2\sum_{\mu\nu}P_{\mu\nu}\left\langle\varphi_\mu(\mathbf{r})\middle|\nabla_{\mathbf{R}_A}V_{\mathrm{loc}}^{\mathrm{PP}}(\mathbf{r})\middle|\varphi_\nu(\mathbf{r})\right\rangle\\
&\qquad+2\sum_{\mu\nu}P_{\mu\nu}\left\langle\varphi_\mu(\mathbf{r})\middle|\nabla_{\mathbf{R}_A}V_{\mathrm{nl}}^{\mathrm{PP}}(\mathbf{r},\mathbf{r}')\middle|\varphi_\nu(\mathbf{r}')\right\rangle \quad .
\end{aligned} \tag{A7}$$

In this case of the Hartree energy and the XC energy the expression is a bit lengthy due to the implicit position dependence in the one-centre charge densities:

$$\begin{aligned}
&\frac{\mathrm{d}}{\mathrm{d}\mathbf{R}_A}(E_{\mathrm{H}}[\{\mathbf{R}_B\},n]+E_{\mathrm{XC}}[\{\mathbf{R}_B\},n])\\
&\quad= 2\sum_{\mu\nu}P_{\mu\nu}\left\langle\tilde{\varphi}_\mu\middle|V_{\mathrm{H}}\left[\tilde{n}+\tilde{n}^0\right]+V_{\mathrm{XC}}[\tilde{n}]\middle|\nabla_{\mathbf{R}_A}\tilde{\varphi}_\nu\right\rangle_{\Omega_{\mathrm{FFT}}}\\
&\qquad+2\sum_{\mu\nu}P_{\mu\nu}\left\langle\tilde{\varphi}_\mu\middle|V_{\mathrm{H}}\left[n^0-\tilde{n}^0\right]\middle|\nabla_{\mathbf{R}_A}\tilde{\varphi}_\nu\right\rangle\\
&\qquad+2\sum_{B}\sum_{\mu\nu\,bc}C'_{b\mu}P_{\mu\nu}\left(\nabla_{\mathbf{R}_A}C'_{cv}\right)\\
&\qquad\times\left\{\left\langle g_b\middle|V_{\mathrm{H}}\left[n_A^1+n_A^{\mathrm{Z}}\right]\middle|g_c\right\rangle+\left\langle g_b\middle|V_{\mathrm{XC}}\left[n_A^1\right]\middle|g_c\right\rangle_{\Omega_{\mathrm{A}}}\right\}\\
&\qquad-2\sum_{B}\sum_{\mu\nu\,bc}\tilde{C}'_{b\mu}P_{\mu\nu}\left(\nabla_{\mathbf{R}_A}\tilde{C}'_{cv}\right)\\
&\qquad\times\left\{\left\langle g_b\middle|V_{\mathrm{H}}\left[\tilde{n}_A^1+n_A^0\right]\middle|g_c\right\rangle+\left\langle g_b\middle|V_{\mathrm{XC}}\left[\tilde{n}_A^1\right]\middle|g_c\right\}\right\rangle_{\Omega_{\mathrm{A}}}\right\}\\
&\qquad+\sum_{A\ell m}\sum_{\mu\nu}P_{\mu\nu}q^{\ell m}\left[\chi_\mu\chi_\nu-\tilde{\chi}_\mu\tilde{\chi}_\nu\right]\\
&\qquad\times\left\{\int\limits_{\Omega_{\mathrm{FFT}}}V_{\mathrm{H}}\left[\tilde{n}+\tilde{n}^0\right]\nabla_{\mathbf{R}_A}\tilde{g}_A^{\ell m}\right.\\
&\qquad+\int V_{\mathrm{H}}[\tilde{n}]\left(\nabla_{\mathbf{R}_A}g_A^{\ell m}-\nabla_{\mathbf{R}_A}\tilde{g}_A^{\ell m}\right)\\
&\qquad\left.+\sum_{A'}\int V_{\mathrm{H}}\left[n_{A'}^0\right]\nabla_{\mathbf{R}_A}g_A^{\ell m}-\sum_{A'}\int V_{\mathrm{H}}\left[\tilde{n}_{A'}^0\right]\nabla_{\mathbf{R}_A}\tilde{g}_A^{\ell m}\right\}\\
&\qquad+2\sum_{A\ell m}\sum_{\mu\nu}P_{\mu\nu}q^{\ell m}\left[\chi_\mu\nabla_{\mathbf{R}_A}\chi_\nu-\tilde{\chi}_\mu\nabla_{\mathbf{R}_A}\tilde{\chi}_\nu\right]\\
&\qquad\times\left\{\int\limits_{\Omega_{\mathrm{FFT}}}V_{\mathrm{H}}\left[\tilde{n}+\tilde{n}^0\right]\tilde{g}_A^{\ell m}+\int V_{\mathrm{H}}[\tilde{n}]\left(g_A^{\ell m}-\tilde{g}_A^{\ell m}\right)\right.\\
&\qquad+\sum_{A'}\int V_{\mathrm{H}}\left[n_{A'}^0\right]g_A^{\ell m}-\sum_{A'}\int V_{\mathrm{H}}\left[\tilde{n}_{A'}^0\right]\tilde{g}_A^{\ell m}\\
&\qquad\left.+\int V_{\mathrm{H}}\left[\tilde{n}_A^1+n_A^0\right]g_A^{\ell m}\right\} \quad .
\end{aligned} \tag{A8}$$

Again, the indices Ω_{FFT} and Ω_{A} denote integration on the FFT grid or on atomic Lebedev grids, respectively.

References

1. Parr RG, Yang W (1989) Density-functional theory of atoms and molecules. Oxford University Press, Oxford
2. Sambe H, Felton RH (1975) J Chem Phys 62: 1122
3. (a) Dunlap BI, Connolly JWD, Sabin JR (1979) J Chem Phys 71: 3396; (b) Dunlap BI, Connolly JWD, Sabin JR (1979) J Chem Phys 71: 4993
4. Lippert G, Hutter J, Parrinello M (1997) Mol Phys 92: 477
5. Ordejón E, Artacho P, Soler JM (1996) Phys Rev B 53: R10441
6. Blöchl PE (1994) Phys Rev B 50: 17953
7. Hohenberg P, Kohn W (1964) Phys Rev B 136: 864
8. Kohn W, Sham LJ (1965) Phys Rev A 140: 1133
9. Lippert G, Hutter J, Ballone P, Parrinello M (1996) J Phys Chem 100: 6231
10. Goedecker S, Teter M, Hutter J (1996) Phys Rev B 54: 1703
11. Hartwigsen C, Goedecker S, Hutter J (1998) Phys Rev B 54: 1703
12. Obara S, Saika A (1986) J Chem Phys 84: 3963
13. Galli G, Parrinello M (1991) In: Pontikis V, Meyer M (eds) Computer simulations in materials science. Proceedings NATO ASI. Kluwer, Dordrecht, p 283
14. Ihm J, Zunger A, Cohen ML (1979) J Phys C 12: 4409
15. Barnett RN, Landman U, Nitzan A, Rajagopal G (1991) J Chem Phys 94: 608
16. Hockney RW (1970) Methods Comput Phys 9: 136
17. Blöchl PE (1995) J Chem Phys 103: 7422
18. Martyna GJ, Tuckerman ME J Chem Phys (1999) 110: 2810
19. Slater JC (1937) Phys Rev 51: 846
20. Lippert G (1997) PhD thesis. Universität Stuttgart
21. Lebedev VI (1975) Zh Vychisl Mat Mat Fiz 15: 48
22. Lebedev VI (1976) Zh Vychisl Mat Mat Fiz 16: 293
23. Lebedev VI (1977) Sib Mat Zh 18: 132
24. Frisch MJ, Trucks GW, Schlegel HB, Gill PMW, Johnson BG, Robb MA, Cheeseman JR, Keith T, Petersson GA, Montgomery JA, Raghavachari K, Al-Laham MA, Zakrzewski VG, Ortiz JV, Foresman JB, Peng CY, Ayala PY, Chen W, Wong MW, Andres JL, Replogle ES, Gomperts R, Martin RL, Fox DJ, Binkley JS, Defrees DJ, Baker J, Stewart JP, Head-Gordon M, Gonzalez C, Pople JA (1995) Gaussian 94, revision B.2. Gaussian, Pittsburgh Pa
25. Hutter J, Ballone P, Bernasconi M, Focher P, Fois E, Goedecker S, Marx D, Parrinello M, Tuckerman M (1995–1996) CPMD, version 3.0. Max-Planck-Institut für Festkörperforschung, Stuttgart, and IBM Zurich Research Laboratory
26. Dickson RM, Becke AD (1993) J Chem Phys 99: 3898
27. Dolphin D (ed) (1978–1979) The porphyrins, vols 1–7. Academic Press, New York
28. (a) (1987) Structure and bonding, vol 64. Springer, Berlin Heidelberg New York; (b) (1991) Structure and bonding, vol 74. Springer, Berlin Heidelberg New York; (c) (1995) Structure and bonding, vol 84. Springer, Berlin Heidelberg New York
29. Momenteau M, Reed CA, (1994) Chem Rev 94: 659

30. Rovira C, Kunc K, Hutter J, Ballone P, Parrinello M (1997) J Phys Chem 101: 8914
31. Becke AD (1986) J Chem Phys 84: 4524
32. Perdew JP (1986) Phys Rev B 33: 8822
33. Mauri F, Galli G, Car R (1993) Phys Rev B 47: 9973
34. Goedecker S (1995) J Comput Phys 118: 261
35. Li XP, Nunes W, Vanderbilt D (1993) Phys Rev B 47: 10891
36. Yang W (1991) Phys Rev Lett 66: 1438
37. Ordéjon, Drabold D, Grumbach M, Martin R (1993) Phys Rev B 48: 14646
38. Boys SF, Bernardi F (1970) Mol Phys 19: 553
39. Peng S-M, Ibers JA (1976) J Am Chem Soc 98: 8032